26.12.5 Convergence of Taylor Maps: Performance of Lower-Order Polynomial Approximations

We close this section with illustrations of the performances of $\mathcal{M}_3$ and $\mathcal{M}_5$, third and fifth order polynomial approximations (including parameter dependence) to the exact map $\mathcal{M}$. All expansions are made about the point (12.12). Comparison of these performances gives some feeling for the convergence properties of the Taylor approximation to $\mathcal{M}$.

Performance of $\mathcal{M}_3$

Figure 33 shows the $\mathcal{M}_3$ counterpart to Figure 24 produced using $\mathcal{M}_8$. Evidently the qualitative features of the period doubling cascade are the same. Also, we have found that there is not qualitative agreement if $\mathcal{M}_2$ is used. We conjecture that generically third-order information is necessary and sufficient to obtain qualitative agreement for a period doubling cascade arising from what once was a period-one fixed point.

Note also that $\mathcal{M}_3$ does not reproduce the three features near $\omega = 1.265$ seen in Figure 25.8.6 for the exact $\mathcal{M}$ and in Figure 24 for $\mathcal{M}_8$. We have found that these features first appear for $\mathcal{M}_n$ when $n = 5$. They belong to what was initially a period-three fixed point for $\mathcal{M}$.

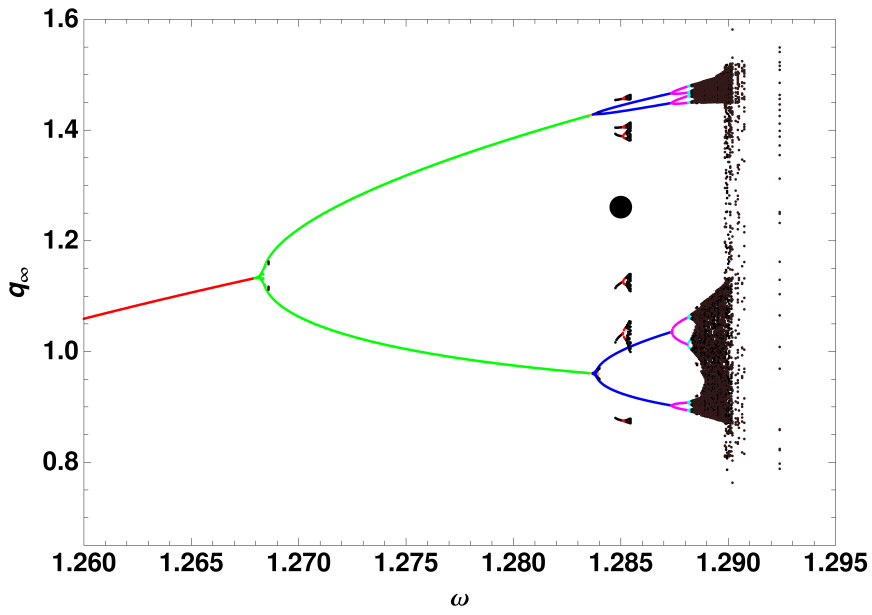

Figure 26.12.33: Partial Feigenbaum diagram for the map $\mathcal{M}_3$. The black dot marks the point about which $\mathcal{M}$ is expanded to yield $\mathcal{M}_3$

.

Figures 34 and 35 show the $\mathcal{M}_3$ counterparts to Figures 26 and 27 produced using $\mathcal{M}_8$.

Evidently there is qualitative agreement. The attractors in Figures 34 and 26 look similar. And, when enlarged, both show evidence of fractal structure. Compare Figures 35 and 27.

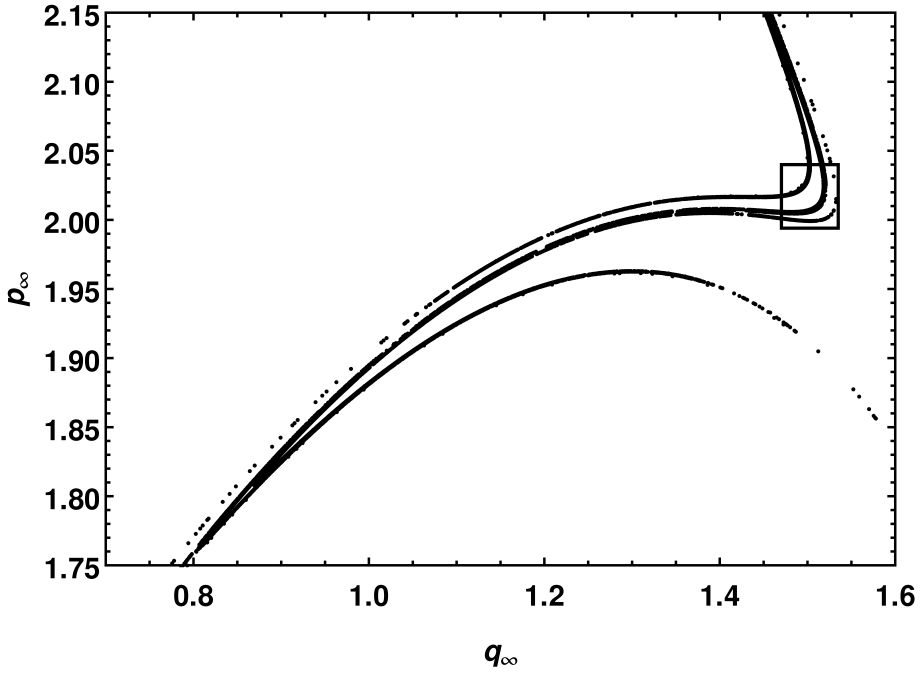

Figure 26.12.34: Limiting values of q_∞, p_∞ for the map $\mathcal{M}_3$ when $\omega = 1.2902$. They appear to lie on a strange attractor.

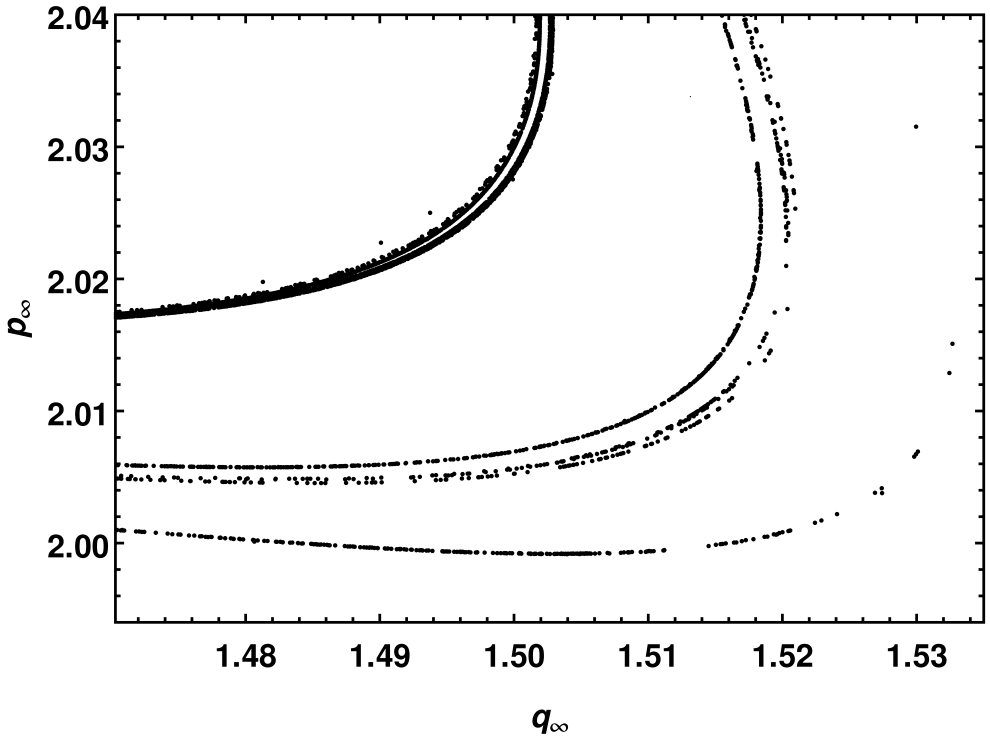

Figure 26.12.35: Enlargement of boxed portion of Figure 34 illustrating the beginning of self-similar fractal structure.

Performance of $\mathcal{M}_5$

Figure 36 shows the $\mathcal{M}_5$ counterpart to Figure 24 produced using $\mathcal{M}_8$. Now there is improved quantitative agreement as well as qualitative agreement. Also, there are now three features near $\omega = 1.265$ that resemble those seen in Figures 25.8.6 and 24.

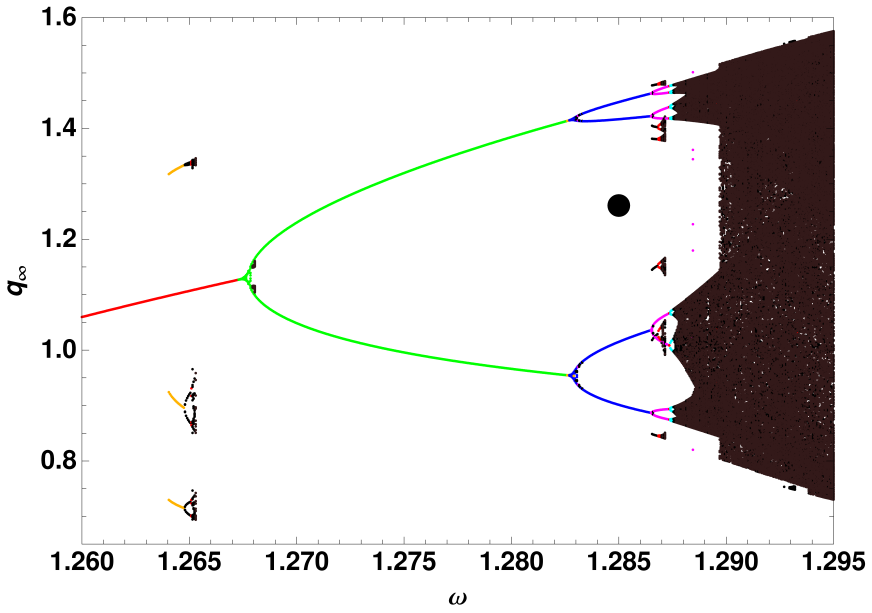

Figure 26.12.36: Partial Feigenbaum diagram for the map $\mathcal{M}_5$. The black dot marks the point about which $\mathcal{M}$ is expanded to yield $\mathcal{M}_5$

.

Figures 37 and 38 show the $\mathcal{M}_5$ counterparts to Figures 26 and 27 produced using $\mathcal{M}_8$. Again there is improved quantitative agreement. We surmise that, for the region of phase space and ω range displayed, convergence appears to be well underway.

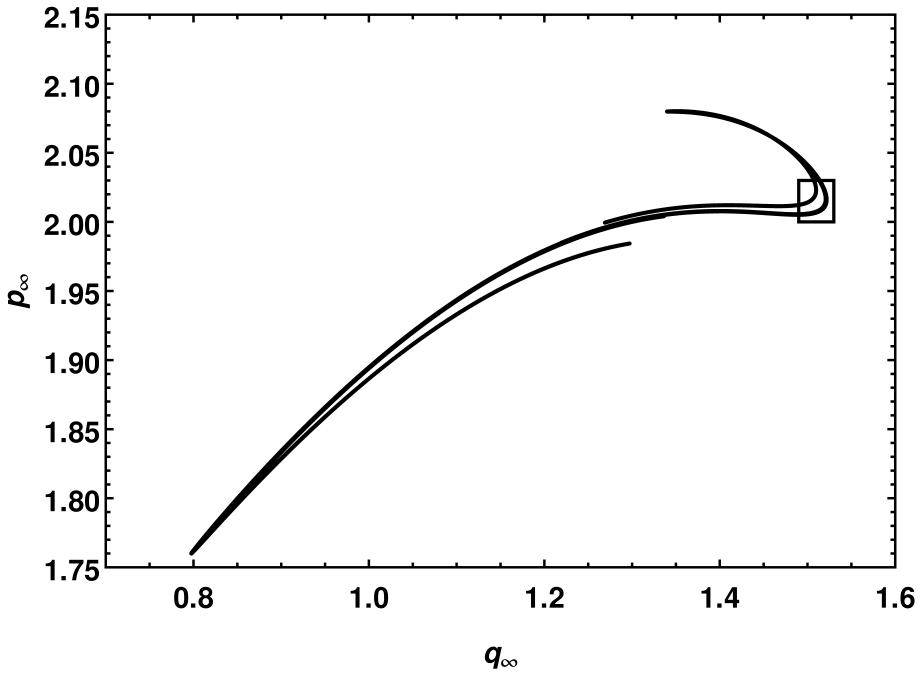

Figure 26.12.37: Limiting values of q_∞, p_∞ for the map $\mathcal{M}_5$ when $\omega = 1.2902$. They appear to lie on a strange attractor.

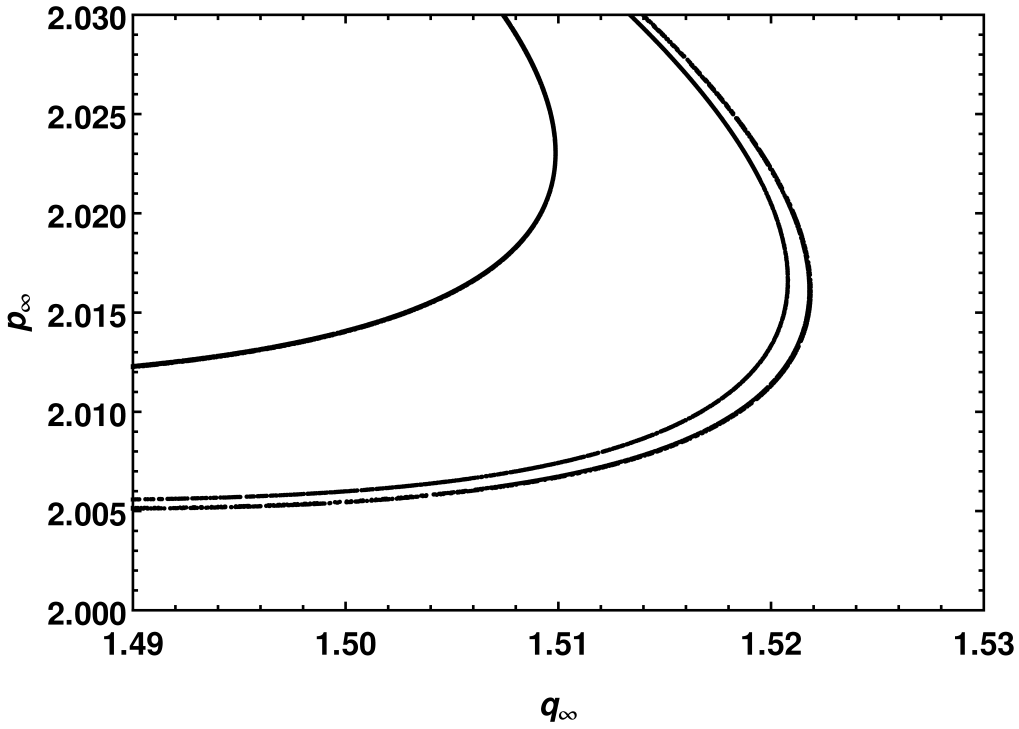

Figure 26.12.38: Enlargement of boxed portion of Figure 37 illustrating the beginning of self-similar fractal structure.

26.12.6 Concluding Summary and Discussion

Poincaré analyticity (and its generalization to include parameter dependence) implies that transfer maps $\mathcal{M}$ arising from ordinary differential equations can be expanded as Taylor series in the initial conditions and also in whatever parameters may be present. Section 10.10 described the complete variational equations, and described how the determination of these expansions is equivalent to solving the complete variational equations. Chapter 25 provided an overview of the properties of the stroboscopic transfer map $\mathcal{M}$ for the Duffing equation. The present section described examples of how n^{th} degree approximations $\mathcal{M}_n$ to $\mathcal{M}$ (including parameter dependence) could reproduce various features of the exact $\mathcal{M}$. In particular it illustrated, remarkably, that $\mathcal{M}_8$ produced an infinite period doubling cascade and apparent strange attractor that closely resembled those of the exact map. It also illustrated how the accuracy of $\mathcal{M}_n$ improves with increasing n.

We have seen that there are situations in which a truncated Taylor map well reproduces results obtained by the integration of differential equations. This is comforting since the behavior of polynomial maps, because such maps can easily be evaluated repeatedly, is often studied in detail with the hope that the behavior of such maps is illustrative of what can be expected for maps in general, including the maps that arise from integrating differential equations.

In view of this success, one might wonder if there are situations in which the use of truncated Taylor maps could replace or at least complement direct numerical integration. There is, of course, the question of convergence for Taylor series, and the convergence domain is related to the (generally unknown) singularity structure of the solution to the differential equation in the complex domain. See Section 35.3. However, if satisfactory approximation can be illustrated by the comparison of numerical integration results with truncated Taylor results for representative solutions in some domain, then the use of truncated Taylor maps to find additional results may be faster than continued numerical integration.

For example, in the case of the Duffing equation, although the determination of the relevant $h_a^r(t)$ of Subsection 10.10.1 requires the simultaneous numerical integration of a large number of differential equations, these equations need be integrated over only one drive period. Once the truncated Taylor series stroboscopic map has been found, its evaluation for any phase-space point and any parameter value is essentially free. All that is required is the evaluation of two n-degree polynomials (one for ζ_1^f and one for ζ_2^f, the deviation variables associated with q^f and p^f, respectively) in three variables (ζ_1^i, ζ_2^i, and ζ_3^i). (Again see Subsection 10.10.1 for notation.) By contrast, the direct construction of a Feigenbaum diagram requires the integration of the Duffing equation for a large number of drive periods and a large number of parameter values. And, determination of the strange attractor associated with the Duffing equation requires the integration of the Duffing equation over thousands of drive periods.

Suppose T_2 is the time required to integrate two equations over a drive period. In our example, it is the time required to integrate the Duffing pair of differential equations (1.4.32) over one drive period. Suppose T_{N_e} is the time required to integrate N_e equations over one drive period. Let $L(m, n)$ be the number of monomials of degree 0 through n in m variables.

It is given by the binomial coefficient

$$L(m,n) = \binom{m+n}{n}. \tag{26.12.14}$$

See Section 7.10. When working with m variables through terms of degree n, the number N_e of differential equations to be integrated to determine the relevant functions $h_a^r(t)$ is given by the relation

$$N_e = mL(m,n), \tag{26.12.15}$$

which amounts to

$$N_e = 3L(3,8) = 3 \times 165 = 495 \tag{26.12.16}$$

in the case of $\mathcal{M}_8$ for the Duffing equation including parameter dependence. We have found in our numerical studies that there is the approximate scaling relation

$$T_{N_e} \simeq (N_e/2)T_2 \tag{26.12.17}$$

for $n \leq 9$. That is, the computation time scales with the number of equations to be integrated. We conclude that in this example the use of $\mathcal{M}_8$ becomes advantageous once the number of drive periods times the number of parameter values exceeds $495/2 \simeq 250$.

With regard to providing complementary information, it is common practice to integrate the first degree variational equations in order to establish the *linear* stability of solutions. Integration of the higher degree variational equations, including possible parameter dependence, provides information about *nonlinear* behavior/stability. As examples, such information is required for the control of orbits in accelerators and the understanding and control of aberrations in optical systems.

In conclusion, there are applications for which use of the higher degree variational equations is advantageous, and the whole subject of the usefulness of truncated Taylor maps merits continued study.

26.12.7 Acknowledgment

Dobrin Kaltchev made major contributions to the work of this section.

26.13 Analytic Properties of Fixed Points and Eigenvalues

As described in the beginning of Section 24.12, integrating analytic differential equations can be expected to yield analytic maps. For these maps we can compute fixed points and the eigenvalues of the linear parts of these maps about their fixed points. What can be said about the parameter dependence of these fixed points and eigenvalues?

Consider first the behavior of eigenvalues. They are roots of the characteristic polynomial (3.4.1) when M is the linear part of the map. The coefficients of this polynomial depend on the matrix elements of M in an analytic way. See Exercise 3.7.14. Moreover, since M is determined by integrating the variational equations, we may expect these matrix elements